POLITECNICO DI TORINO
Repository ISTITUZIONALE

Solar-driven CO2 reduction catalysed by hybrid supramolecular photocathodes and enhanced by ionic liquids

Original
Solar-driven CO2 reduction catalysed by hybrid supramolecular photocathodes and enhanced by ionic liquids / Miro, R., Guzman Medina, H., Godard, C., Gual, A., Zammillo, F., Schubert, T.J.S., Iliev, B., Chiodoni, A., Hernandez, S., de los Bernardos, M.D.. - In: JOURNAL OF ADVANCED CATALYSIS SCIENCE AND TECHNOLOGY. - ISSN 2408-9834. - 13:6(2023), pp. 1708-1717. [10.1039/d2cy01523d]

Availability:
This version is available at: 11583/2977454 since: 2024-01-17T12:18:21Z

Publisher:
Royal Society of Chemistry ACS

Published
DOI:10.1039/d2cy01523d

Terms of use:

This article is made available under terms and conditions as specified in the corresponding bibliographic description in the repository

Publisher copyright

(Article begins on next page)

16 September 2026

Catalysis Science & Technology

ROYAL SOCIETY OF CHEMISTRY

PAPER

View Article Online
View Journal

Check for updates

Cite this: DOI: 10.1039/d2cy01523d

Solar-driven CO_2 reduction catalysed by hybrid supramolecular photocathodes and enhanced by ionic liquids†

Roger Miró, [a] Hilmar Guzmán, [b] Cyril Godard, *[c] Aitor Gual, *[a] Federica Zammillo, [b] Thomas J. S. Schubert, [d] Boyan Iliev, [d] Angelica Chiodoni, [e] Simelys Hernández *[b] and Miriam Díaz de los Bernardos *[a]

Photoelectrochemical carbon dioxide reduction (CO_2) at ambient temperature and pressure was performed using molecular chromophores and catalyst assemblies on $CuGaO_2$-based electrodes in an ionic liquid (IL) organic solution, acting as a CO_2 absorbent and electrolyte. A simple and versatile methodology based on the silanization of the $CuGaO_2$ electrode followed by electropolymerization provided a series of molecular and supramolecular hybrid photocathodes for solar driven CO_2 reduction. Focusing on the cathodic half reactions, the most promising conditions for the formation of CO_2 reduction products were determined. The results revealed a beneficial effect of the ionic liquid on the conversion of CO_2 to formic acid and suppression of the production of hydrogen. The potentiality of anchoring supramolecular complexes on semiconductor photoelectrocatalysts was demonstrated to boost both carrier transport and catalytic activity with a FE_{red} of up to 81% compared with the obtained FE_{red} of 52% using bare $CuGaO_2$ with formate as the major product.

Received 29th August 2022,
Accepted 13th February 2023

DOI: 10.1039/d2cy01523d

rsc.li/catalysis

Open Access Article. Published on 15 February 2023. Downloaded on 3/1/2023 6:25:30 PM.
This article is licensed under a Creative Commons Attribution 3.0 Unported Licence.

Introduction

Over the last decade, the increase in CO_2 concentration in the atmosphere, which could eventually cause irreversible effects on nature, has triggered much attention in chemical research on carbon capture and utilization (CCU) technologies.[1,2] For *CO_2 capture*, the main challenge is to find an ideal absorbent that exhibits high selectivity and high capacity for CO_2. In this context, ionic liquids (ILs) have demonstrated excellent capture capacity for CO_2;[3] in addition, they have also been widely adopted as electrolytes in the electrochemical conversion of CO_2 since they exhibit a high CO_2 solubility, low vapor pressure, high ionic conductivity and wide electrochemical windows.[4] Furthermore, it was reported that ILs can interact with CO_2 to decrease the overpotential and enhance the product selectivity.[5] CO_2 electroreduction studies also demonstrated that appropriate combinations of ILs and catalysts can enhance the generation of CO with faradaic efficiencies of up to 96%.[6–8] Among the IL structures, 1-butyl-3-methylimidazolium triflate (BMIM·TfO) is a promising structure due to its high CO_2 solubility (0.6–0.8 mol CO_2 per mol_{IL}).[9] Therefore, although it has not been often used as an electrolyte for the CO_2 reduction reaction (CO_2RR), herein it will be exploited instead of the most commonly employed BMIM·BF_4, to avoid the issues related to the latter like the hydrolysis of the $[BF_4]^-$ and the possible formation of HF under electrochemical CO_2RR conditions.[10]

Regarding *CO_2 conversion*, the main challenge is to efficiently activate and reduce CO_2 to reach the zero-carbon footprint goal. In this respect, visible-light-driven CO_2 reduction in combination with water oxidation is a promising solution as it involves the use of abundant water and inexhaustible solar energy, and constitutes one of the most representative models of artificial photosynthesis.[11] Molecular metal complexes and semiconductors are promising candidate photocatalysts, which can reduce CO_2 to CO, formic acid, formaldehyde or other hydrocarbons.[12] Although both molecular metal complexes and semiconductors have strengths and weaknesses, their main limitations (*i.e.* low oxidation ability, low selectivity for reduction reactions and stability issues) can be overcome *via* the construction of suitable molecule/semiconductor hybrid

[a] *Eurecat, Technology Centre of Catalonia, Unit of Chemical Technologies, Tarragona, 43007, Spain. E-mail: miriam.diaz@eurecat.org*
[b] *CREST Group, Department of Applied Science and Technology (DISAT), Politecnico di Torino, Turin, Italy*
[c] *Departament de Química Física i Inorgànica, Universitat Rovira i Virgili, Tarragona, 43007, Spain*
[d] *Iolitec Ionic Liquids Technology GmbH, Heilbronn, 74076, Germany*
[e] *Center for Sustainable Future Technologies (IIT@Polito), Italian Institute of Technology, Turin, Italy*

† Electronic supplementary information (ESI) available. See DOI: https://doi.org/10.1039/d2cy01523d

Open Access Article. Published on 15 February 2023. Downloaded on 3/1/2023 6:25:30 PM.
This article is licensed under a Creative Commons Attribution 3.0 Unported Licence.

materials. In this approach, the efficient electron transfer from a semiconductor to an immobilized molecular catalyst and the suppression of back electron transfer are crucial for reducing CO_2 on the molecule/semiconductor hybrid material.[13] To this end, both the conduction band potential of the semiconductor and the reduction potential of the molecular unit should be carefully designed.

Supramolecular hybrid photocatalysts based on ruthenium (Ru(II))–rhenium (Re(I)) complexes were reported to efficiently catalyze CO_2 photoreduction under visible light with faradaic efficiencies of up to 87% with CO and HCOOH as the major products.[12,13] Osamu Ishitani and co-workers developed a hybrid photocathode based on $CuGaO_2$ and a supramolecular Ru–Re complex immobilized using phosphonic acid as an anchoring group.[14] This system allowed them to obtain faradaic efficiencies of up to 81% with a $CO:H_2$ ratio of 1.5 : 1 and to exceed the performance observed with a NiO electrode; however, the instability of the phosphonic acid anchoring group was the main drawback. Later, Meyer and co-workers adopted a new immobilization method based on the silanization of NiO, followed by electropolymerization of a molecular Ru complex and a molecular Re complex, thereby improving the overall energy conversion efficiency and the system stability during long-term operation, for up to 10 hours.[15] Recently, Osamu Ishitani and co-workers performed a new immobilization process by the electropolymerization of a supramolecular Ru–Ru catalyst, obtaining a robust and selective system to CO and HCOOH for CO_2 reduction coupled with water oxidation, which remained stable for 100 h with a total faradaic efficiency of 65%.[16]

Inspired by the progress in capture and conversion of CO_2 demonstrated using ILs and given the results achieved with the different semiconductors and immobilization procedures, we report here the preparation of various hybrid assemblies based on $CuGaO_2$ and a series of new molecular and supramolecular Ru and Re complexes. The photoelectrocatalytic CO_2 reduction was carried out using BMIM·TfO as a catholyte and a i) Ru(II) photosensitizer complex ($\mathbf{Ru_{VLA}}$) co-immobilized with a Re(I) catalyst complex ($\mathbf{Re_{CAT}}$), ii) supramolecular **RuRe1** complex and iii) binuclear **RuRe2** complex to compare the electron transfer efficiency using the different supramolecular complexes. Higher performance was achieved with the supramolecular and binuclear systems than with the co-immobilized complexes and the results revealed the beneficial role of the ionic liquid in promoting the conversion of CO_2 into formic acid and C_{2+} alcohols, while improving the stability of the system and suppressing the production of H_2.

Results and discussion

Synthesis and characterization of $CuGaO_2$ and $CuGaO_2$-VTES

X-ray diffraction analysis confirmed the successful synthesis of the $CuGaO_2$ structure without other obvious impurity phases. The diffraction pattern (see ESI† Fig. S1) was in agreement with the typical delafossite structure with a hexagonal unit cell.[17] The calculated unit cell parameters were 2.974 and 17.143 Å for a and c, respectively, with a crystallite size of 58.0 ± 1.1 nm calculated by the Scherrer formula. These values agree well with the JCPDS data (a = 2.977, c = 17.171 Å, JCPDS database 77-2495) of $CuGaO_2$.[17] The FESEM image (Fig. 1) of the obtained solid displays the surface morphology of the $CuGaO_2$ particles, which exhibit a few micrometers in size with parallel lines on the surface indicating their laminar structure. Moreover, the energy dispersive X-ray analysis of the sample (see ESI† Fig. S2) confirmed the average Cu : Ga : O ratio of 1 : 1 : 2.

The functionalized $CuGaO_2$ ($CuGaO_2$-VTES) catalyst was analyzed with FESEM-EDX (see Fig. S3 and S4†), which indicated that the morphology remains unchanged after functionalization while EDX analysis confirmed the presence of Si with an approximate Cu : Si ratio of 16 : 1.

Synthesis and characterization of Ru and Re molecular complexes

Four new Ru and Re molecular complexes containing a **bpy-V** ligand were successfully synthesized in high yield and characterized by NMR, MS, IR and UV-vis spectroscopy (Fig. 2).

The synthesis of the $\mathbf{Re_{CAT}}$ complex was performed using $Re(CO)_5Br$ as a precursor. This Re precursor and one equivalent of **bpy-V** ligand were dissolved in toluene and heated under reflux overnight to substitute two CO ligands, forming the $\mathbf{Re_{CAT}}$ complex in high isolated yield (84%).

For the synthesis of $\mathbf{Ru_{VLA}}$, the $[Ru(COD)Cl_2]$ precursor was first prepared starting from $RuCl_3{\cdot}3H_2O$; then, the COD ligand was substituted by two 4,4′-dimethyl-2,2′-bipyridine ($bpyMe_2$) ligands in 1,2-dichlorobenzene at 155 °C, obtaining the $[Ru(bpyMe_2)Cl_2]$ complex. Finally, the remaining chloride ligands were substituted by one **bpy-V** ligand in an acetone/water solution obtaining the final desired complex in 74% isolated yield.

The complexes **RuRe1** and **RuRe2** were synthesized following the same synthetic strategy as the one adopted for $\mathbf{Ru_{VLA}}$. The distance effect between Ru and Re was studied using these two complexes containing different bridge ligands between the Ru and Re. First, the $[Ru(COD)Cl_2]$ precursor was prepared, followed by the replacement of the COD ligand with two **bpy-V** ligands, obtaining the [Ru(bpy-V)Cl_2] complex. Then, the chloride ligands were replaced by a

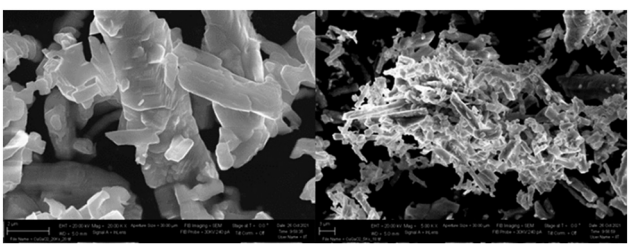

Fig. 1 FESEM images of the synthesized $CuGaO_2$.

This journal is © The Royal Society of Chemistry 2023

Open Access Article. Published on 15 February 2023. Downloaded on 3/1/2023 6:25:30 PM.
This article is licensed under a Creative Commons Attribution 3.0 Unported Licence.

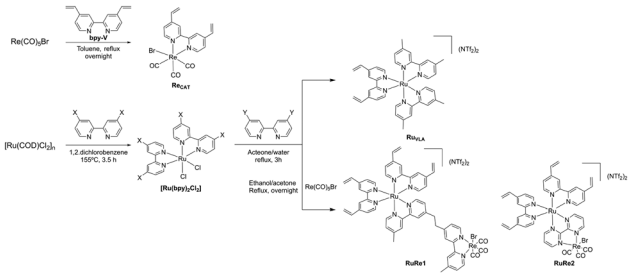

Fig. 2 Schematic representation of the synthesis of the Ru and Re complexes used in this study.

1,2-bis(4′-methyl-[2,2′-bipyridin]-4-yl)ethane or 2,2′-bipyrimidine ligand to obtain the corresponding Ru complexes. Finally, a reaction with one equivalent of $Re(CO)_5$-Br complex under reflux yielded the final **RuRe1** and **RuRe2** complexes in good isolated yields (64% and 67%, respectively). The coordination of the Re complex was confirmed by IR spectroscopy *via* the detection of the characteristic vibration bands of the CO ligands. The ^{1}H and ^{13}C NMR and HRMS analyses confirmed the structure of these complexes (see the ESI† for the detailed synthetic description and characterization of all the complexes).

Preparation of the RuRe@$CuGaO_2$ photocathodes

Three photoelectrodes were prepared by electropolymerization of the synthesized homogeneous complexes (Fig. 2). The efficiency of the electropolymerization procedure of $CuGaO_2$-VTES with the molecular complexes was corroborated by the continuous enhancement of the current densities after each scan (see ESI† S19). This observation suggested the *in situ* formation of polymeric layers onto the surface of the electrode. Furthermore, the presence of multiple vinyl groups in the diverse Ru and Re complexes led to a final layer-by-layer assembly of polymers, which translates into a different combination of interconnected complexes with the achievement of a high molecular loading on the surface of the electrodes.[15,18]

The immobilization of Ru and Re species onto $CuGaO_2$-VTES was supported by FESEM-EDX analysis. The obtained semi-quantitative results, the average of three different electrode zones, suggested the anchoring of equimolar amounts of Ru and Re species for both supramolecular Ru–Re complexes, whereas 2 moles of Re per mole of Ru were measured for the mixture of homogeneous complexes (see Table 1).

An estimation of the relative amount of Ru and Re immobilized with respect to the Cu deposited onto the support was performed to determine the efficiency of the anchoring approach. The approach used in the present work allowed a higher immobilization of the **RuRe1** complex than that of the **RuRe2** complex. Moreover, through the FESEM images, agglomerations were evidenced in all the electrodes containing the RuRe1 molecular complex (see Fig. 3).

The region containing the agglomeration (Fig. 3a) was analyzed by EDX and revealed a higher content of Ru and Re (Fig. 3b). These EDX results confirm that the agglomeration consists in **RuRe1** supramolecular complexes interconnected between them. The line scanning EDX (Fig. 3c) performed in both regions, the agglomerated and non-agglomerated one, also confirms the presence of a higher content of Ru and Re in the agglomerated region compared to the non-agglomerated ones. Since the **RuRe1** complex contains four anchoring groups, the coupling between molecular complexes could explain the agglomeration with high Ru and Re contents.

UV-visible absorption spectra of all the prepared electrodes were measured in diffuse reflectance mode (Fig. 4). The UV-vis spectrum of the bare $CuGaO_2$ indicates no absorption in the visible range.[17,19] However, a change was observed with the introduction of the Ru and Re complexes. Indeed, the electrode containing the molecular $\mathbf{Ru_{VLA}}$ and $\mathbf{Re_{CAT}}$ complexes immobilized separately exhibited a small absorption band which starts at λ = 550 nm. Meanwhile, the electrode containing **RuRe1** showed a large absorption band starting at λ = 600 nm and that with **RuRe2** showed an absorption band throughout the visible light spectrum. These results are in concordance with previous reports where a characteristic peak appeared in the UV spectrum at around 464 nm, attributed to the singlet metal-to-ligand-charge-transfer absorption band of the Ru complex.[18]

Photoelectrochemical characterization of $CuGaO_2$

There is a literature discussion about the electro- and photoelectrochemical activity of $CuGaO_2$ in the CO_2 reduction reaction.[14,19] The photoelectrochemical and electrochemical properties of the bare $CuGaO_2$ were first studied under dark conditions and under simulated sunlight irradiation. The current-potential curves (Fig. 5a) show a difference in the current between the dark and light conditions indicating that $CuGaO_2$ is photocatalytically active under sunlight irradiation in a 0.3 M BMIM·TfO acetonitrile solution saturated with CO_2. Indeed, from −0.3 to −1.2 V *vs.* Ag/AgCl, a difference in

Table 1 Average of approximated amounts of Ru and Re on the surface of the electrode analyzed by EDX

Electrode	Ratio of Cu : Ru[a]	Ratio of Cu : Re[b]	Ratio of Ru : Re
Ru + Re@$CuGaO_2$	39 : 1 (0.16)	19 : 1 (0.32)	1 : 2
RuRe1@$CuGaO_2$	1.6 : 1 (3.78)	1.5 : 1 (4.03)	1 : 1.1
RuRe2@$CuGaO_2$	26 : 1 (0.23)	23 : 1 (0.26)	1 : 1.1

[a] In brackets, value in μmol_{Ru} cm^{-2}. [b] In brackets, value in μmol_{Re} cm^{-2}.

Open Access Article. Published on 15 February 2023. Downloaded on 3/1/2023 6:25:30 PM.
This article is licensed under a Creative Commons Attribution 3.0 Unported Licence.

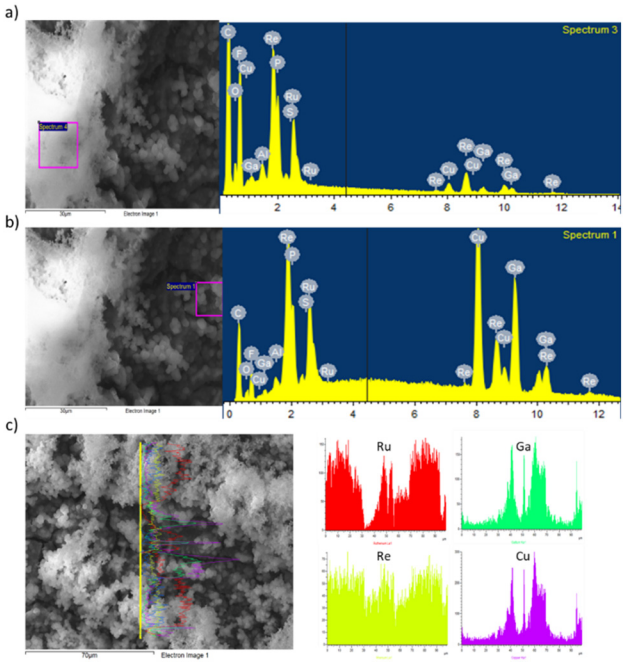

Fig. 3 FESEM images and EDX analysis of the **RuRe1@CuGaO$_2$** electrode. a) EDX analysis of a region in the agglomeration section. b) EDX analysis of a region without agglomeration. c) Line scanning EDX analysis.

the current density values of about 19 μA cm^{-2} between darkness and light irradiation can be observed.

Chopped dark/light chronoamperometry performed at −2.0 V (Fig. 5b) confirms the CuGaO$_2$ photoactivity, showing an average photocurrent contribution of −0.195 mA cm^{-2}.

Photoelectrochemical reduction of CO_2 using the $CuGaO_2$ photocathode

The effect of light and current intensity on the CO_2 reduction performance was investigated on $CuGaO_2$ by performing a

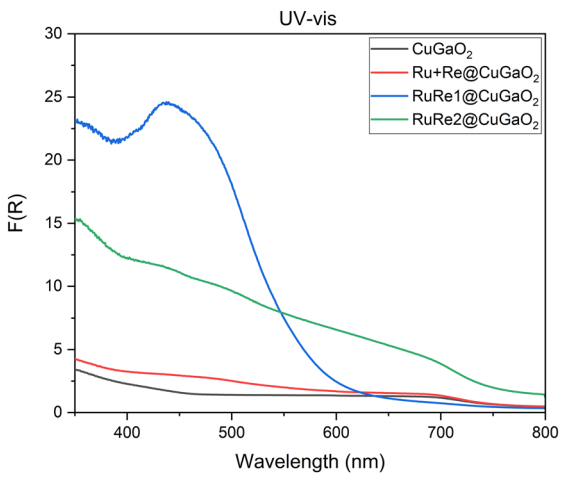

Fig. 4 Diffuse-reflectance UV-visible absorption spectra of the prepared electrodes.

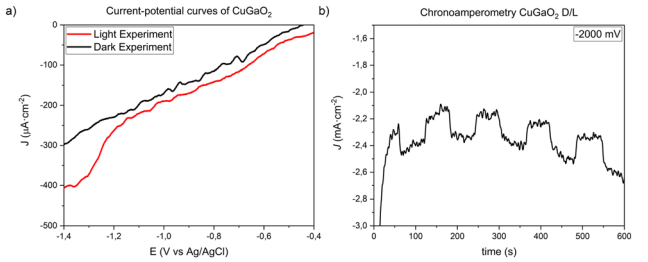

Fig. 5 a) Current–potential curves of the synthesized $CuGaO_2$ with and without simulated sunlight irradiation in CO_2 saturated 0.3 M BMIM·TfO acetonitrile solution. b) Dark/light chronoamperometry of $CuGaO_2$ performed at −2.0 V *vs.* Ag/AgCl under the same conditions as those in a).

current screening under both light and dark conditions and analyzing the gas and liquid products in each experiment. Short chronopotentiometry experiments of 30 min were performed: based on cyclic voltammetry (see ESI† Fig. S27), different current intensities were applied, specifically −0.2, −1.5, −3, −6, −10 and −20 mA cm^{-2}, with the aim to observe the CO_2 reduction product behavior in each experiment.

As can be observed in Fig. 6, a significant difference was highlighted between dark and light conditions. Under dark conditions, a major selectivity towards CO_2 reduction products and a faradaic efficiency to H_2 lower than 10% were obtained. In contrast, under simulated sunlight irradiation

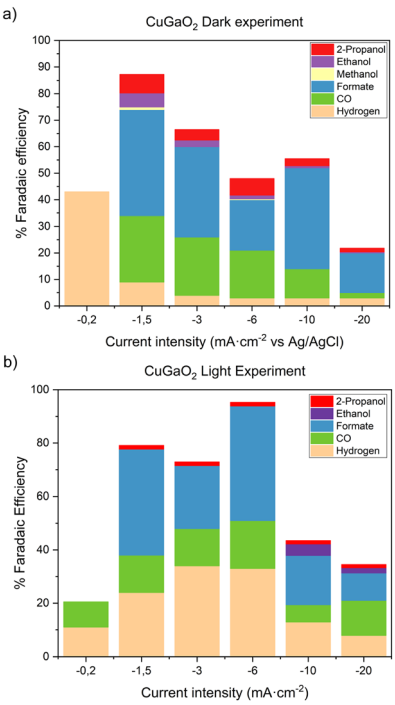

Fig. 6 Faradaic efficiencies of gas and liquid products produced in 30 min chronopotentiometry measurements at different current intensities on $CuGaO_2$ electrodes in a CO_2 saturated 0.3 M BMIM·TfO acetonitrile solution. a) Experiment without simulated sunlight irradiation. b) Experiment under simulated sunlight irradiation.

This journal is © The Royal Society of Chemistry 2023

Open Access Article. Published on 15 February 2023. Downloaded on 3/1/2023 6:25:30 PM.
This article is licensed under a Creative Commons Attribution 3.0 Unported Licence.

conditions, a substantial increase in hydrogen production was observed. In both cases, the total faradaic efficiency decreased when higher current densities were applied. This behavior was attributed to the instability of the catalyst, *i.e.*, self-reduction of $CuGaO_2$.[20]

Under both dark and light conditions, formate was the major CO_2 reduction product, followed by CO. Small quantities of propanol, ethanol, and methanol were also detected. The production of CO and H_2 was monitored during the experiment and was stable during the time of chronopotentiometry.

Fig. 7 shows the comparison of the chronopotentiometry measurements between dark and light conditions. The chronopotentiometry measurements performed at the same current intensity under visible light irradiation (dashed line) and in the dark (solid line) revealed a difference in the corresponding potential values. In general, lower potential values (in absolute values) were measured under light conditions than in the dark. However, the opposite behavior was observed when the chronopotentiometry was performed at −10 and −20 mA cm^{-2}.

Chronopotentiometry (CP) experiments for 120 minutes were performed in the dark and under visible light irradiation by applying −1.5 mA cm^{-2} to evaluate the stability of the CO_2RR over time with the $CuGaO_2$ bare material. At short reaction times, CO was the main product. However, at longer reaction times, the CO production decreased under both dark and light conditions (Fig. 8). When the experiment was performed in the dark, a constant decrease of CO selectivity was observed along with a constant increase in H_2 production. Under light irradiation, the CO production decreased more rapidly and after *ca.* 40 min, H_2 became the main product. The results obtained show that the total faradaic efficiencies are higher in the dark (FE_{total} = 71% in the dark *vs.* 52% under light), confirming the quick deactivation of the bare $CuGaO_2$ under light irradiation. These results were in agreement with previously reported data.[19]

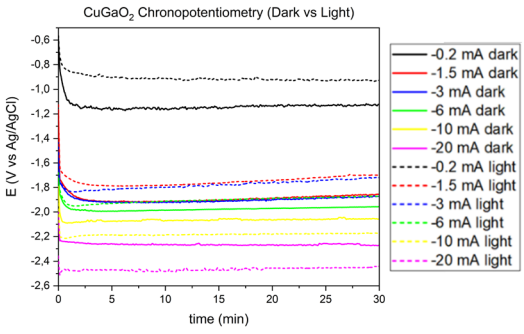

Fig. 7 Chronopotentiometry curves applying different current intensities under light irradiation (dashed line) and in the dark (solid line) on $CuGaO_2$ electrodes in a CO_2 saturated 0.3 M BMIM·TfO acetonitrile solution. The line colors are the same for the chronopotentiometry measurements performed at the same current intensity.

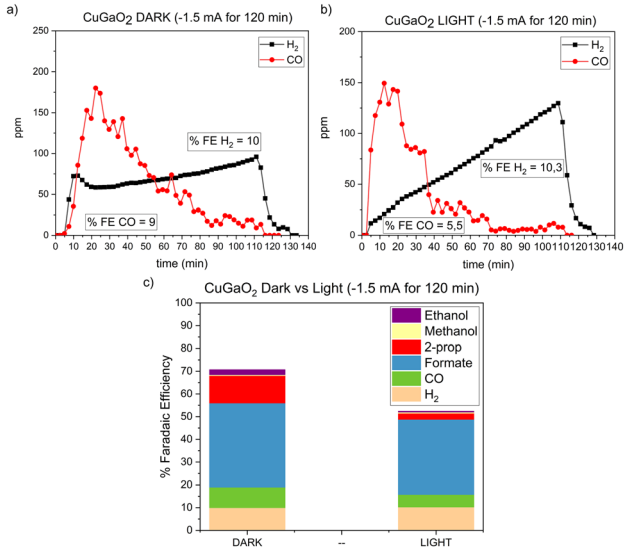

Fig. 8 Chronopotentiometry performed at −1.5 mA cm^{-2} for 120 min in 0.3 M BMIM·TfO acetonitrile solution saturated with CO_2. a) CO and H_2 production under dark conditions. b) CO and H_2 production under light conditions. c) Faradaic efficiencies under dark and light conditions.

Photoelectrochemical properties of Ru + Re@$CuGaO_2$

The photoelectrochemical properties of the prepared $CuGaO_2$ electrode bearing a mixture of $\mathbf{Ru_{VLA}}$ and $\mathbf{Re_{CAT}}$ (**Ru + Re@$CuGaO_2$**) were studied and compared with those of the bare $CuGaO_2$ electrode. The experiments were performed using simulated sunlight irradiation in an acetonitrile solution containing 0.3 M of BMIM·TfO and saturated with CO_2. The current–potential curves (Fig. 9a) show a difference in the current response between dark and light conditions. Interestingly, **Ru + Re@$CuGaO_2$** exhibited an approximate current difference of 32 μA cm^{-2}, which constituted a higher photo-response than using the bare $CuGaO_2$ (19 μA cm^{-2}) and indicated that the higher photocurrent was induced by the injection of electrons from $CuGaO_2$ to the Ru photosensitizer.

Dark/light chronoamperometry performed at −2.0 V (Fig. 9b) confirmed the activity under light irradiation of the

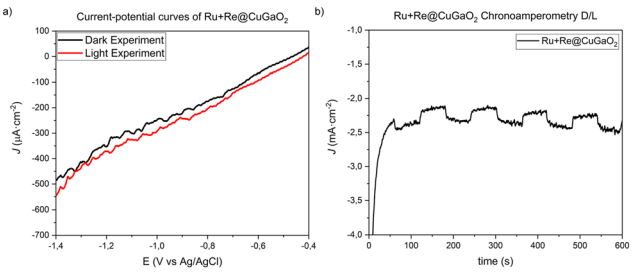

Fig. 9 a) Current–potential curves of the synthesized **Ru + Re@$CuGaO_2$** with and without light irradiation. b) Dark/light chronoamperometry of the **Ru + Re@$CuGaO_2$** electrode performed at −2.0 V *vs.* Ag/AgCl in a CO_2 saturated 0.3 M BMIM·TfO acetonitrile solution.

Open Access Article. Published on 15 February 2023. Downloaded on 3/1/2023 6:25:30 PM.
This article is licensed under a Creative Commons Attribution 3.0 Unported Licence.

Ru + Re@CuGaO$_2$ photocathode, showing an average photocurrent contribution of −0.204 mA cm^{-2} in a CO_2 saturated 0.3 M BMIM·TfO acetonitrile solution. A comparison between Fig. 5b and 9b evidence that the two photoelectrodes gave a similar average photocurrent contribution at this fixed potential value. Nonetheless, **Ru + Re@CuGaO$_2$** was revealed to be more stable over time.

Photoelectrochemical reduction of CO_2 using the Ru + Re@CuGaO$_2$ photocathode

The selectivity of the **Ru + Re@CuGaO$_2$** electrode for the CO_2-RR was evaluated under simulated sunlight irradiation. As for the bare $CuGaO_2$, short chronopotentiometry experiments of 30 min were performed by applying different constant current densities: −0.2, −1.5, −3, −6, −10 and −20 mA cm^{-2}, respectively. The results are displayed in Fig. 10.

In general, the formation of CO_2 reduction products was enhanced by the immobilization of Ru and Re molecular complexes onto the $CuGaO_2$ semiconductor. More specifically, at current density values lower than −10 mA cm^{-2}, the H_2 production decreased along with an increase in the selectivity to CO_2 reduction products. It should be noted that with the **Ru + Re@CuGaO$_2$** electrode, a total faradaic efficiency of 99% was reached at −1.5 mA cm^{-2}, with a FE_{H2} of only 7%. A detrimental effect was evidenced at more negative currents with a clear decrease in the total FE, which could be due to the catalyst modification under these conditions. In view of these results, a current value of −1.5 mA cm^{-2} was selected for conducting the subsequent analyses. A blank control experiment was carried out using the **Ru + Re@CuGaO$_2$** electrode in a N_2 saturated 0.3 M BMIM·TfO acetonitrile solution. After applying −1.5 mA cm^{-2} for 30 min, any CO_2 reduction product was detected, confirming that the products originate from CO_2.

Next, the effect of the reaction medium was evaluated. The reactions were carried out in the following CO_2 saturated solutions: (i) 0.3 M BMIM·TfO in acetonitrile, chosen in view of the good results obtained using this IL in some recent studies,[6–8] (ii) 0.3 M Et_4N·PF_6 in acetonitrile, to compare the use of an IL to that of a simple quaternary ammonium salt,[21,22] and (iii) an aqueous solution of 0.1 M $KHCO_3$, which was selected as a typical aqueous electrolyte.[23]

In aqueous medium, a constant H_2 production was obtained with a total FE of 80% including a FE to formate (the main CO_2-RR product) of 14% (Fig. 11). As could be expected, in organic media (acetonitrile solutions of BMIM·TfO and Et_4N·PF_6), a higher selectivity to CO_2 reduction products was obtained with formate as the major product. Interestingly, C_{2+} products like ethanol and propanol were also promoted in the organic solvents, and in particular with the IL electrolyte. This suggests the role of the imidazolium and ammonium-based electrolytes as co-catalysts that may also influence the CO_2RR mechanism. Indeed, C_{2+} product formation requires the co-presence of adsorbed CO (CO*) and CH_x (CH_x^*) intermediates, which react by CO*–CO*dimerization or CO*–CH_x^* coupling at the catalyst surface.[24]

Comparing the chronoamperometry curves, the experiment performed using acetonitrile 0.3 M BMIM·TfO as an electrolyte revealed a stable voltage of −1.9 V *vs.* Ag/AgCl (Fig. 12a), whereas using 0.3 M Et_4N·PF_6 in acetonitrile resulted in a variation of the voltage along the potential window from −1.8 V to −1.6 V. Using the aqueous solution of 0.1 M $KHCO_3$, a stable voltage at −1.6 V *vs.* Ag/AgCl was also observed. It should be highlighted that the potential associated with the experiments seems to correlate with the product selectivity, since high hydrogen faradaic efficiencies and low formate faradaic efficiencies were achieved in the aqueous solution of 0.1 M $KHCO_3$ at −1.6 V, whereas the opposite trend was observed using 0.3 M BMIM·TfO in acetonitrile as the electrolyte at −1.9 V. In the case of 0.3 M Et_4N·PF_6 in acetonitrile as the electrolyte, the selectivity varied with the potential along the experiment. In fact, considering the H_2 and CO production during the test when using Et_4N·PF_6 (Fig. 12b), the CO production decreased severely after 40 min with a concomitant increase in hydrogen production.

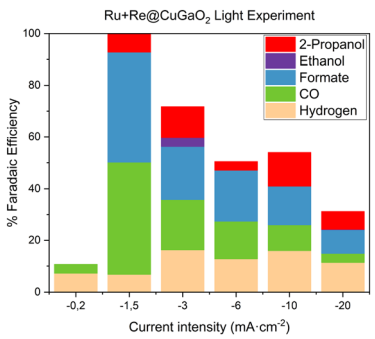

Fig. 10 Faradaic efficiencies of gas and liquid products produced in 30 min chronopotentiometry at different current intensities in a 0.3 M BMIM·TfO acetonitrile solution saturated with CO_2 under simulated sunlight irradiation with the **Ru + Re@CuGaO$_2$** electrode.

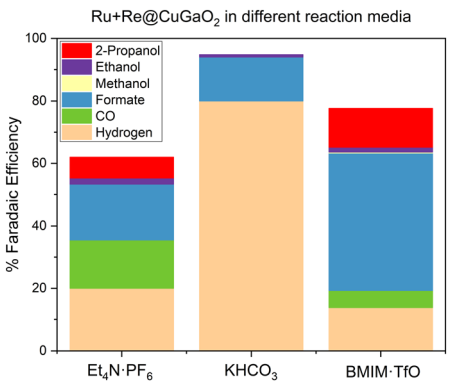

Fig. 11 Faradaic efficiencies of gas and liquid products produced in 120 min chronopotentiometry at −1.5 mA cm^{-2}, under continuous simulated sunlight irradiation, using different electrolytes, 0.3 M Et_4N·PF_6 in acetonitrile, 0.1 M $KHCO_3$ in H_2O and 0.3 M BMIM·TfO in acetonitrile, all saturated with CO_2.

This journal is © The Royal Society of Chemistry 2023

Open Access Article. Published on 15 February 2023. Downloaded on 3/1/2023 6:25:30 PM. This article is licensed under a Creative Commons Attribution 3.0 Unported Licence.

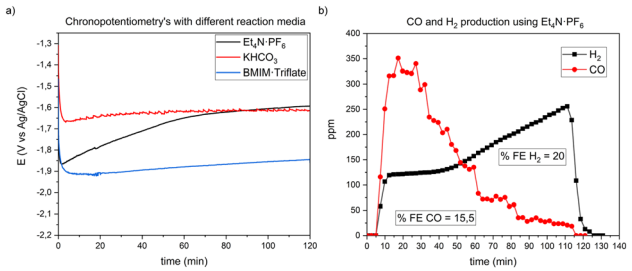

Fig. 12 a) 120 min chronopotentiometry using the **Ru + Re@CuGaO$_2$** catalyst applying −1.5 mA cm^{-2} under simulated sunlight irradiation in a CO_2 saturated solution using different reaction media. b) CO and H_2 production during the 120 min chronopotentiometry using the **Ru + Re@CuGaO$_2$** catalyst at −1.5 mA cm^{-2} under the same conditions as those in a) using 0.3 M $Et_4N{\cdot}PF_6$ in acetonitrile as an electrolyte.

Based on these results, the beneficial effect of BMIM·TfO as the electrolyte was attributed to the high CO_2 solubility[9] and its potential role in lowering the activation energy of CO_2 reduction.[25] Then, 0.3 M BMIM·TfO in acetonitrile was selected as the electrolyte to study the immobilization of the different molecular complexes synthesized onto the $CuGaO_2$ semiconductor.

Ru and Re complex effect in the photoelectrochemical reduction of CO_2 in ionic liquid

The current–potential curves under dark and light irradiation conditions and the chopped chronoamperometry curves for the **RuRe1@CuGaO$_2$** and **RuRe2@CuGaO$_2$** materials are displayed in Fig. 13.

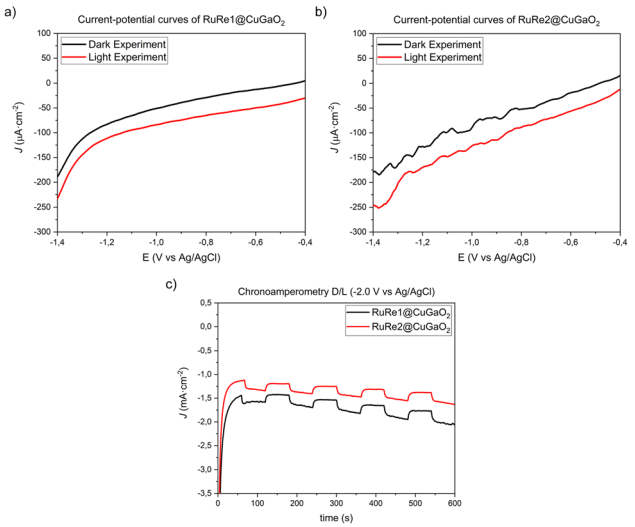

Fig. 13 Current–potential curves with and without light irradiation in CO_2 saturated 0.3 M BMIM·TfO acetonitrile solution of the a) **RuRe1@CuGaO$_2$** electrode and b) **RuRe2@CuGaO$_2$** electrode. c) Dark/light chronoamperometry of **RuRe1@CuGaO$_2$** (red line) and **RuRe2@CuGaO$_2$** (blue line) performed at −2.0 V *vs.* Ag/AgCl in 0.3 M BMIM·TfO acetonitrile solution saturated with CO_2.

In both cases, a difference in the current response between dark and light conditions was observed (Fig. 13). Slight differences in the measured photocurrent were observed for the electrodes containing the supramolecular complexes: **RuRe1@CuGaO$_2$** provided an average photocurrent of 36 μA cm^{-2} and **RuRe2@CuGaO$_2$** showed a value of 37 μA cm^{-2}, from −0.4 to −1.2 V *vs.* Ag/AgCl. However, both electrodes exhibited a higher photoactivity than **Ru + Re@CuGaO$_2$** (with an average photocurrent of 32 μA cm^{-2} from −0.4 to −1.2 V *vs.* Ag/AgCl).

Nevertheless, when dark/light chronoamperometry at −2.0 V was performed (Fig. 13c), the electrodes containing the supramolecular complexes showed a lower average photocurrent contribution, −0.156 (**RuRe1@CuGaO$_2$**) and −0.150 mA cm^{-2} (**RuRe2@CuGaO$_2$**), than the **Ru + Re@CuGaO$_2$** electrode, −0.204 mA cm^{-2}.

Subsequently, the effect of the different Ru/Re complexes on the CO_2 photoelectroreduction selectivity were evaluated during 120 min chronopotentiometry by applying −1.5 mA cm^{-2} under simulated sunlight conditions. In Fig. 14a, the faradaic efficiencies of the gaseous and liquid products for each catalyst at this current density value are displayed. Using the bare $CuGaO_2$ electrode, a low total faradaic efficiency was obtained (52%). With all the prepared hybrid materials, an increase in the faradaic efficiency was observed up to 81%, which evidenced the protective and stabilizing role of the Ru and Re complexes that hinder the $CuGaO_2$ modification. Among them, similar faradaic efficiencies for H_2 and CO_2RR products were obtained; however, with the **RuRe1** and **RuRe2** complexes, lower external potentials were necessary at the same current intensity, which evidenced a higher generated photovoltage and a more efficient electron transfer when using the supramolecular systems rather than immobilizing separately the **Ru$_{VLA}$** and **Re$_{CAT}$** complexes (Fig. 14b), which is in agreement with their superior UV-vis light absorption. Using the hybrid materials, a higher faradaic efficiency to formic acid was obtained compared with that of the bare $CuGaO_2$, *ca.* 45% *vs.* 30%, respectively. Interestingly, the ethanol production and propanol

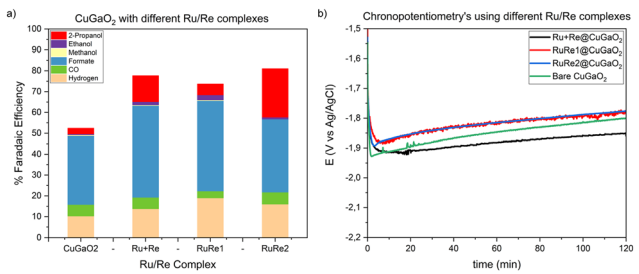

Fig. 14 a) Faradaic efficiencies of gas and liquid products produced in 120 min chronopotentiometry tests at −1.5 mA cm^{-2}, under continuous simulated sunlight irradiation in a 0.3 M BMI·TfO CO_2 saturated acetonitrile solution using different Ru and Re complexes. b) 120 min chronopotentiometry recorded curves applying −1.5 mA cm^{-2} under the same conditions as those in a) using different Ru and Re complexes.

Open Access Article. Published on 15 February 2023. Downloaded on 3/1/2023 6:25:30 PM.
This article is licensed under a Creative Commons Attribution 3.0 Unported Licence.

production were enhanced with the hybrid materials and in particular with the binuclear **RuRe2** complex. As previously mentioned, such results highlight the role of the Ru and Re complexes in co-catalyzing the multi-electron processes subsequent to the formate and CO formation at the catalyst surface.

Moreover, the hybrid materials synthesized in this work not only enhanced the faradaic efficiency of the process but also showed higher stability than the bare $CuGaO_2$. Finally, the stability of the hybrid materials was corroborated by analyzing the electrodes after the CP experiments by FESEM-EDX. A similar morphology of the hybrid materials was observed after the CP experiments, indicating a positive effect of the immobilization of the molecular complexes (see the ESI†). Additionally, the semi-quantitative results obtained by EDX (Table 2) suggested the similar loading of the Ru and Re species before and after the CP experiments, thus confirming the stability of these systems under the reported reaction conditions.

Experimental section

Synthesis and functionalization of $CuGaO_2$

The synthesis of the $CuGaO_2$ metal oxide was carried out using a solid state reaction procedure adapted from the literature.[14] A mixture of Cu_2O (1.76 mmol, 251.9 mg, Sigma-Aldrich, 99.99% purity) and Ga_2O_3 (1.76 mmol, 330.0 mg, Sigma-Aldrich, 99.99% purity) powders was heated up from room temperature to 1100 °C at 5 °C min^{-1} under a N_2 flow. Then the mixture was maintained for 15 h at 1100 °C and finally cooled down to room temperature under a N_2 flow.

The synthesized $CuGaO_2$ was then functionalized with vinyltriethoxysilane (VTES) by adding 0.1 g of $CuGaO_2$ to a 20 mL solution of isopropanol containing 10 mM vinyltriethoxysilane. The dispersion was stirred overnight at room temperature, then filtered, and finally washed with isopropanol.

Synthesis of molecular Ru and Re complexes

Four new complexes with 2,2′-bipyridine containing vinyl groups in the *para*-position (**bpy-V**) were synthesized in this work: (i) Re CO_2 reduction co-catalyst ($\mathbf{Re_{CAT}}$); (ii) Ru visible light absorber ($\mathbf{Ru_{VLA}}$); (iii) supramolecular Ru–Re complex (**RuRe1**) and (iv) the binuclear Ru–Re (**RuRe2**) complex. The synthesis of the $\mathbf{Re_{CAT}}$ complex was adapted from a reported procedure[26] but using the **bpy-V** ligand. The synthesis of the $\mathbf{Ru_{VLA}}$, **RuRe1** and **RuRe2** materials was instead performed according to another procedure.[18,27] The detailed synthetic procedures for these complexes are described in the ESI.†

RuRe@$CuGaO_2$ photocathode preparation

The electrodes were manufactured by airbrushing a catalytic ink onto a porous carbon support (Toray carbon paper 060, from FuelCellStore).[28] The catalytic ink was constituted by various components: (i) the $CuGaO_2$-VTES catalyst in powder form; (ii) NAFION® (dispersion, 5 wt% in water and 1-propanol, from Sigma Aldrich) as a binder for the particles and ionomer, and (iii) ethanol (from Sigma Aldrich), as a carrier for the ink deposition, since the ink must be fluid to be uniformly spread on the area of interest. Each $CuGaO_2$-VTES electrode was prepared with a geometric area of 1 cm^2 and a catalyst loading of 1 mg cm^{-2}. The deposition process was performed by placing carbon paper on a heating plate at 50 °C to ensure complete solvent evaporation. A pressure of 1.5 bar for the carrier gas (nitrogen) in the airbrush inlet was selected to have a continuous ink flow, avoiding undesired liquid drops. All the electrodes were then kept on the heating plate for 15 min before their use.

Next, the prepared electrodes containing $CuGaO_2$-VTES were subjected to electropolymerization of the corresponding molecular complexes.[15] The electropolymerization of the complexes was performed employing a three electrode set-up with $CuGaO_2$-VTES, a platinum wire and $Ag/AgNO_3$ as the working, counter, and reference electrodes, respectively. The electrodes were submerged in an argon degassed acetonitrile solution containing the corresponding complex at a 0.5 mM concentration and tetraethylammonium hexafluorophosphate ($Et_4N{\cdot}PF_6$, 0.1 M) as an electrolyte. Cyclic voltammetry measurements were performed from 0 to −1.9 V *vs.* $Ag/AgNO_3$ and the applied voltage was scanned multiple times with a scan rate of 100 mV s^{-1}. After 60 scans, the electrode was removed and washed with acetonitrile. Three different photoelectrodes were prepared by immobilizing a series of homogeneous complexes onto $CuGaO_2$-VTES: (i) Ru visible light absorber complex and Re CO_2 reduction catalyst complex co-immobilized (**Ru + Re@$CuGaO_2$**), (ii) supramolecular Ru–Re complex (**RuRe1@$CuGaO_2$**) and (iii) binuclear Ru–Re complex (**RuRe2@$CuGaO_2$**).

Characterization

The physicochemical properties of the synthesized $CuGaO_2$ catalysts and of the electrodes prepared by electropolymerization were analyzed by X-ray diffraction (XRD, Panalytical X'Pert PRO diffractometer) and with Field

Table 2 Average amounts of Ru and Re on the surface of the electrode analyzed by EDX before (first value) and after (second value) the CP experiments

Electrode	Ratio of Cu : Ru	Ratio of Cu : Re	Ratio of Ru : Re
Ru + Re@$CuGaO_2$	39 : 1/40 : 1	19 : 1/22 : 1	1 : 2/1 : 1.8
RuRe1@$CuGaO_2$	1.6 : 1/2.3 : 1	1.5 : 1/2.5 : 1	1 : 1.1/1 : 1.1
RuRe2@$CuGaO_2$	26 : 1/33 : 1	23 : 1/43 : 1	1 : 1.1/1 : 1.3

This journal is © The Royal Society of Chemistry 2023

Open Access Article. Published on 15 February 2023. Downloaded on 3/1/2023 6:25:30 PM.
This article is licensed under a Creative Commons Attribution 3.0 Unported Licence.

Emission Scanning Electron Microscopy (FESEM) with Energy Dispersive X-ray Spectroscopy (ZEISS Auriga, equipped with an OXFORD X-MAX EDS detector). The electrodes were analyzed before and after the CO_2RR tests to confirm the presence of Ru and Re and to determine the morphology and the approximate content of the complexes. UV-vis reflectance spectra ($F(R) = (1 - R)^2/2R$: Kubelka–Munk function) of the prepared electrodes were collected with a spectrophotometer (Varian Cary 5000 spectrophotometer).

The molecular complexes were characterized by ^{1}H and ^{13}C NMR (Varian Mercury VX 400), HRMS (Agilent Time-of-Flight 6210 using ESI-TOF), FT-IR (Bruker Vertex-70 instrument with attenuated total reflectance) and UV-vis (UV-1800 Shimadzu apparatus).

Photoelectrochemical measurements

The photoelectrochemical (PEC) measurements were performed in an H-type cell (made of quartz) with a three-electrode configuration. In a typical test, the anodic chamber was equipped with 28 mL of a 0.1 M KOH aqueous solution and a Pt mesh as the counter electrode. The cathodic chamber was instead equipped with 50 mL of 0.3 M BMIM·TfO acetonitrile solution (except when another electrolyte is specified), Ag/AgCl (KCl sat.) as the reference electrode and a $CuGaO_2$-based electrode as the working electrode. The cathodic and anodic chambers were separated by a Fumasep® FBM bipolar exchange membrane (from FUMATECH BWT GmbH). Prior to each measurement, the electrolyte solution was purged for 20 min with a nitrogen (N_2) flow rate of 20 mL min^{-1} to remove the oxygen present in the solution. Afterwards, the solution was saturated for 20 min under a CO_2 flow rate of 20 mL min^{-1}. During the experiments, a constant CO_2 flow rate of 20 mL min^{-1} was maintained.

The PEC measurements were carried out with a Voltalab potentiostat (from Radiometer Analytical SAS). Linear sweep voltammetry (LSV) and cyclic voltammetry curves were recorded in the dark and under continuous or chopped simulated solar light illumination conditions, in the range between −0.20 and −2.2 V *vs.* Ag/AgCl (KCl sat.) (with a sweep rate of 20 mV s^{-1}). Chronoamperometry (CA) measurements were performed at −2.0 V *vs.* Ag/AgCl (KCl sat.) over 1 min darkness and 1 min simulated irradiation intervals. Chronopotentiometry (CP) measurements were performed both in the dark and under continuous simulated solar light irradiation conditions by using a Newport 450 W Xe lamp equipped with an AM 1.5 G filter. The H-type cell was illuminated from the cathodic side maintaining the intensity of the light at 1000 W m^{-2} by adjusting the distance between the light source and the PEC cell.

The gas products (H_2 and CO) were determined continuously during all the experiments using a micro gas-chromatograph (Varian 490-GC from Agilent) directly connected to the cell. Samples of the liquid products were analyzed at the beginning and at the end of each experiment, by means of high-performance liquid chromatography (Shimadzu HPLC) and a gas chromatograph (Perkin Elmer GC with a mass spectrometer) with a headspace for the quantification of formate and alcohols, respectively.

Conclusions

A series of four molecular complexes was synthesized and characterized. Three different hybrid materials were prepared with the synthesized molecular complexes and their photoelectrocatalytic CO_2 reduction performance was tested in the BMIM·TfO ionic liquid. An electropolymerization process was used for the first time for the immobilization of supramolecular Ru–Re complexes on VTES-modified $CuGaO_2$. A comparison of the co-immobilization procedure of the separate $\mathbf{Ru_{VLA}}$ and $\mathbf{Re_{CAT}}$ complexes with the supramolecular **RuRe1** and the binuclear **RuRe2** complexes demonstrated an enhanced photovoltage generation and electron transfer when the supramolecular and binuclear complexes were used. The potential of the approach of anchoring molecular complexes onto the $CuGaO_2$ photo-electrocatalyst to boost both its carrier transport and catalytic activity with respect to the bare semiconductor material was shown. Furthermore, various electrolytes were evaluated and the use of ionic liquids was demonstrated to enhance both the CO_2 reduction selectivity (by suppressing the H_2 evolution reaction) and the stability of the photo-electrocatalytic performance. The combination of the use of the IL and the hybrid materials at the photocatalyst surface increased the semiconductor stability towards its restructuration, which resulted in a 30% increase of the total faradaic efficiency *vs.* the bare $CuGaO_2$, and in an enhanced formic acid production (from 30% to 45%) as well as C_{2+} alcohol formation. Further investigations will be devoted to investigating the long-term stability and to elucidating the role of the supramolecular and binuclear complexes, and of the IL, in co-catalyzing multi-electron CO_2 reduction reaction pathways under photo-electrochemical conditions.

Conflicts of interest

There are no conflicts to declare.

Acknowledgements

The authors would like to acknowledge the European Union's Horizon 2020 Research and Innovation Programme under grant agreement no. 862192 (SUNCOCHEM project), the Ministerio de Economia y Competividad (PID2019-104427RB-I00) and Eurecat's "Vicente López" PhD grant program for funding.

Notes and references

1 A. Rafiee, K. Rajab Khalilpour, D. Milani and M. Panahi, *J. Environ. Chem. Eng.*, 2018, **6**, 5771–5794.
2 E. Alper and O. Yuksel Orhan, *Petroleum*, 2017, **3**, 109–126.

Open Access Article. Published on 15 February 2023. Downloaded on 3/1/2023 6:25:30 PM.
This article is licensed under a Creative Commons Attribution 3.0 Unported Licence.

3 S. Lian, C. Song, Q. Liu, E. Duan, H. Ren and Y. Kitamura, *J. Environ. Sci.*, 2021, **99**, 281–295.
4 D. R. Macfarlane, M. Forsyth, P. C. Howlett, J. M. Pringle, J. Sun, G. Annat, W. Neil and E. I. Izgorodina, *Acc. Chem. Res.*, 2007, **40**, 1165–1173.
5 J. Feng, S. Zeng, J. Feng, H. Dong and X. Zhang, *Chin. J. Chem.*, 2018, **36**, 961–970.
6 J. Medina-Ramos, J. L. Dimeglio and J. Rosenthal, *J. Am. Chem. Soc.*, 2014, **136**, 8361–8367.
7 J. Medina-Ramos, R. C. Pupillo, T. P. Keane, J. L. Dimeglio and J. Rosenthal, *J. Am. Chem. Soc.*, 2015, **137**, 5021–5027.
8 Z. Zhang, M. Chi, G. M. Veith, P. Zhang, D. A. Lutterman, J. Rosenthal, S. H. Overbury, S. Dai and H. Zhu, *ACS Catal.*, 2016, **6**, 6255–6264.
9 S. N. V. K. Aki, B. R. Mellein, E. M. Saurer and J. F. Brennecke, *J. Phys. Chem. B*, 2004, **108**, 20355–20365.
10 M. G. Freire, C. M. S. S. Neves, I. M. Marrucho and A. P. Coutinho, *J. Phys. Chem. A*, 2010, **114**, 3744–3749.
11 K. E. Dalle, J. Warnan, J. J. Leung, B. Reuillard, I. S. Karmel and E. Reisner, *Chem. Rev.*, 2019, **119**, 2752–2875.
12 B. Zhang and L. Sun, *Chem. Soc. Rev.*, 2019, **48**, 2216–2264.
13 A. Nakada, H. Kumagai, M. Robert, O. Ishitani and K. Maeda, *Acc. Mater. Res.*, 2021, **2**, 458–470.
14 H. Kumagai, G. Sahara, K. Maeda, M. Higashi, R. Abe and O. Ishitani, *Chem. Sci.*, 2017, **8**, 4242–4249.
15 T. T. Li, B. Shan and T. J. Meyer, *ACS Energy Lett.*, 2019, **4**, 629–636.
16 R. Kamata, H. Kumagai, Y. Yamazaki, M. Higashi, R. Abe and O. Ishitani, *J. Mater. Chem. A*, 2021, **9**, 1517–1529.
17 M. Lee, D. Kim, Y. T. Yoon and Y. Il Kim, *Bull. Korean Chem. Soc.*, 2014, **35**, 3261.
18 R. Kamata, H. Kumagai, Y. Yamazaki, G. Sahara and O. Ishitani, *ACS Appl. Mater. Interfaces*, 2019, **11**, 5632–5641.
19 J. W. Lekse, M. K. Underwood, J. P. Lewis and C. Matranga, *J. Phys. Chem. C*, 2012, **116**, 1865–1872.
20 C. Y. Toe, Z. Zheng, H. Wu, J. Scott, R. Amal and Y. H. Ng, *Angew. Chem., Int. Ed.*, 2018, **57**, 13613–13617.
21 J. Choi, T. M. Benedetti, R. Jalili, A. Walker, G. G. Wallace and D. L. Officer, *Chem. – Eur. J.*, 2016, **22**, 14158–14161.
22 A. Khadhraoui, P. Gotico, B. Boitrel, W. Leibl, Z. Halime and A. Aukauloo, *Chem. Commun.*, 2018, **54**, 11630–11633.
23 X. Li, J. Yu, M. Jaroniec and X. Chen, *Chem. Rev.*, 2019, **119**, 3962–4179.
24 H. Guzm, F. Salomone, S. Bensaid, M. Castellino, N. Russo and S. Hern, *ACS Appl. Mater. Interfaces*, 2022, **14**, 517–530.
25 D. Yang, Q. Zhu and B. Han, *Innovation*, 2020, **1**, 100016.
26 M. Braumüller, M. Schulz, M. Staniszewska, D. Sorsche, M. Wunderlin, J. Popp, J. Guthmuller, B. Dietzek and S. Rau, *Dalton Trans.*, 2016, **45**, 9216–9228.
27 K. Sekizawa, K. Maeda, K. Domen, K. Koike and O. Ishitani, *J. Am. Chem. Soc.*, 2013, **135**, 4596–4599.
28 H. Guzmán, F. Zammillo, D. Roldán, C. Galletti, N. Russo and S. Hernández, *Catalysts*, 2021, **11**, 482.

 This journal is © The Royal Society of Chemistry 2023